Jurnal Teknologi Maklumat & Multimedia **8**(2010): 1 - 19

Asymmetry Identification Using Generalised Symmetry Axes

LEILA FAVAEDI & MARIA PETROU

ABSTRACT

We present an algorithm for identifying asymmetry in CT images of the human body, relying on the local reflective axis of symmetry. As asymmetry in such images may be a sign of abnormality, our method compares the two sides of the image divided by the extracted axis of symmetry in order to identify regions of interest. Both, extraction of local axis of symmetry and identification of deformities, are obtained automatically. The algorithm is based on registration and extraction of bone contours to generate the desired symmetry axis. Also, to facilitate comparison of the left side with the reflected right side of the image, the local axis of symmetry is made straight by alignment of the image pixels.

Keywords: Asymmetry, Local Reflective Axis, CT Image.

ABSTRAK

Pengarang membentangkan satu algoritma untuk mengenal pasti imej simetri tubuh manusia dalam imbasan imej CT, dengan berpandukan paksi simetri reflektif setempat. Imej simetri lazimnya, membawa tanda bahawa wujudnya ketidaknormalan, kaedah ini membandingkan dua imej sisi yang dibahagikan kepada paksi ekstrek dengan tujuan untuk mengenal pasti kawasan tidak normal. Kedua-duanya iaitu, pembahagian paksi ekstrek dan pengenalan diformasi, diperoleh secara automatik. Algoritma yang digunakan adalah berasaskan pendaftaran dan ekstraksi kontur tulang untuk menghasilkan paksi simetri yang dikehendaki. Juga, untuk membandingkan imej sebelah kiri yang dipantulkan ke sebelah kanan, paksi reflektif setempat dibuat lurus melalui pelarasan piksel imej.

Kata kunci: Simetri, Paksi Reflekstif Setempat, Imej CT.

INTRODUCTION

Symmetry detection and analysis has been used in various applications in computer vision, ranging from facial image analysis (Mitra & Liu 2004) and vehicle detection (Zeilke et al. 1993), to medical image analysis (Tuzikov et al. 2003; Mancas et al. 2005) and texture discrimination (Bonneh et al. 1993; Chetverikov 1995). In various neurological and plastic surgery applications, the symmetry between two halves of the imaged organ has to be assessed and quantified. There are several researchers who have worked on detecting reflective symmetry in medical images. Alterson and Plewes (Alterson & Plewes 2003) presented a symmetry detection algorithm for breast cancer determination based on feature extraction techniques. Junck et al. (1990) developed a method for automatic detection of line symmetry in brain images based on correlation analysis. Several more algorithms have been proposed to detect the symmetry plane in brain images that may be used for tumor extraction (e.g. (Joshi 2003; Prima 2002; Tuzikov 2003)). Most of the papers concentrate on brain

symmetry. In this paper we are interested in bone symmetries for plastic surgery applications. Bones are best depicted in X-ray-based imaging.

Computer Tomography (CT) images are X-ray based and they are not only used for diagnostic purposes, but also for treatment and surgical planning, and for determining the prognosis for various conditions. In CT images, one may distinguish between different types of tissue, such as bone, muscle and fat. Facial and skull CT scanning is often used when fast surgical diagnosis and planning are vital. The vast majority of facial and head trauma patients with isolated or severe injuries are injured as a result of road traffic accidents, falling, or beating. Internal bleeding, injuries and deformities in these kinds of patients destroy the symmetry, for example, of the frontal view of the face. Although there are many works on finding the reflective symmetry axis in the fields of mathematics, computer vision and image processing, the main problem in many natural objects is that the axis of symmetry is not usually just a straight line, but rather a generalised curve. In this paper, we develop methodology for identifying the breaking of symmetry in CT images of parts of the human body, that are expected to be symmetric, and quantifying the degree of asymmetry, as a diagnostic support tool for surgeons. To quantify asymmetry, first, the symmetry axis between the two halves of the depicted part has to be defined. This may not be a straight line. We refer to such an axis of symmetry as "generalised axis of symmetry". Once the generalised symmetry axis is defined, the differences between the two halves of the depicted part are quantified. Both these stages are fully automated.

To identify the generalised symmetry axis, we start from a gross, straight line estimate and refine it by using sub-part matching. As the applications we are interested in involve structures that may be identified by contours, we use as sub parts the contours identified by the level sets method. Although the majority of our experimental data concern images of the human head, our methodology may be applied to any imaged part of the human body where symmetry is expected. This paper is structured as follows. In section 2 we present our methodology. In section 3 we present some experimental results and we conclude in section 4.

METHODOLOGY

The methodology we propose is fully automatic and consists of several stages.

A. *Level sets method for contour detection*

First, an active contour method [6], which uses a functional similar to the Mumford-Shah functional for segmentation [7] is applied to an input image I of size $M \times N$ to segment the bone contours. Let us assume that $C_0(p) = (x(p), y(p))$, parametrized by p $(0 \le p \le 1)$ is an initial closed contour defined on the image coordinates (x, y). By evolving the contour in the direction of its Euclidean normal vector, using a scalar speed function, a family of curves $C(p, n) = (x(p, n), y(p, n))$ is generated, parametrised by time parameter n. To obtain the bone contours, an energy functional E is defined as

$$E(C_1, C_2, C) = \mu \times \sum_{(x(p)y(p)) \in curve} \left| C_p(p) \right| + \lambda_1 \times \sum_{(i,j) \in inside(C)} \left| I(x_i, y_j) \right|^2 + \lambda_2 \times \sum_{(i,j) \in outside(C)} \left| I(x_i, y_j) - C_2(x_i, y_j) \right|^2 \quad (1)$$

where $I(x, y)$ is the image intensity, μ, $\lambda 1$ and $\lambda 2$ are positive constants, and $C1$ and $C2$ are constant matrices where all their entries are the mean intensities of image I inside and outside curve C, respectively. To find C such that $E(C1, C2, C)$ is minimised, the level set method may be used so that curve C is represented by the zero level set of a signed function $\varphi(x, y, n)$, such that:

$$C_1(x_i, y_j) = \frac{\sum_{i,j \in \varphi \le 0} I(x_i, y_j)}{n} \tag{2}$$

where n is the number of pixels inside the curve, and

$$C_2(x_i, y_j) = \frac{\sum_{i,j \in \varphi > 0} I(x_i, y_j)}{m} \tag{3}$$

where m is the number of pixels outside the curve.

Let us initialise function $\varphi(x, y, n)$ as the signed distance function of each (x, y) point to the nearest curve point. (Function $\varphi(x, y, n)$ takes value 0 on curve $C(p, n) = \{(x, y) | \varphi(x, y, n) = 0\}$) So, by using the Heaviside function H, the Dirac measure δ , the energy function can be rewritten over the entire domain rather than separately inside or outside curve C. The value of φ is negative inside the curve and positive outside the curve. Let us define:

$$H(\varphi) = \begin{cases} 1, & if \quad \varphi \ge 0 \\ 0, & if \quad \varphi < 0 \end{cases}, \quad \delta(\varphi) = \frac{d}{d\varphi} H(\varphi) \tag{4}$$

Then

$$E(C_1, C_2, C) = \mu \times \sum \delta(\varphi(x_i, y_j)) |\nabla \varphi(x_i, y_j)| + \lambda_1 \times \sum |I(x_i, y_j) - C_1(x_i, y_j)|^2 H(\varphi(x_i, y_j)) + \lambda_2 \times \sum |I(x_i, y_j) - C_2(x_i, y_j)|^2 (1 - H(\varphi(x_i, y_j))) \tag{5}$$

where all summations now are over all image pixels.

Then, it can be shown [6], that the evolution of function $\varphi(x, y, n)$ that leads to the minimization of the energy function (5) is given by

$$\frac{\varphi_{i,j}^{n+\Delta n} - \varphi_{i,j}^{n}}{\Delta n} = |\nabla_{i,j} \varphi_{i,j}^{n}| \left[\mu \nabla_{i,j} \cdot \frac{\nabla_{i,j} \varphi_{i,j}^{n}}{|\nabla_{i,j} \varphi_{i,j}^{n}|} - \lambda_1 (I(x_i, y_j) - C_1(x_i, y_j))^2 + \lambda_2 (I(x_i, y_j) - C_2(x_i, y_j))^2 \right] \tag{6}$$

where Δn is the time step and $\varphi^{n}_{i,j} = \varphi(xi, y\,j, n)$. In all experiments we performed, we selected $\Delta n = 0.1$.

So, for every pixel $(xi, y\,j)$, we compute $\varphi^{n+1}_{i,j}$ using

$$\varphi_{i,j}^{n+1} = \varphi_{i,j}^{n} + |\nabla_{i,j} \varphi_{i,j}^{n}| \left[\mu \nabla_{i,j} \cdot \frac{\nabla_{i,j} \varphi_{i,j}^{n}}{|\nabla_{i,j} \varphi_{i,j}^{n}|} - \lambda_1 (I(x_i, y_j) - C_1(x_i - y_j))^2 + \lambda_2 (I(x_i, y_j) - C_2(x_i, y_j))^2 \right] \times 0. \tag{7}$$

where $\nabla_{i,j} \cdot \frac{\nabla_{i,j} \varphi_{i,j}}{|\nabla_{i,j} \varphi_{i,j}|}$ is the curvature of the curve, computed as [18]

$$\nabla_{i,j} \cdot \frac{\nabla_{i,j} \varphi_{i,j}}{|\nabla_{i,j} \varphi_{i,j}|} = \frac{\varphi_{xx} \varphi_y^2 - 2\varphi_{xy} \varphi_x \varphi_y + \varphi_{yy} \varphi_x^2}{(\varphi_x^2 + \varphi_y^2)^{3/2}} \tag{8}$$

where

$$\varphi_{xx} = \frac{\partial^2 \varphi_{i,j}}{\partial x^2} = \varphi_{i+1,j} - 2\varphi_{i,j} + \varphi_{i-1,j}$$

$$\varphi_{yy} = \frac{\partial^2 \varphi_{i,j}}{\partial y^2} = \varphi_{i,j+1} - 2\varphi_{i,j} + \varphi_{i,j-1}$$

$$\varphi_{xy} = \frac{\partial^2 \varphi_{i,j}}{\partial x \partial y} = \frac{\varphi_{i+1,j+1} - \varphi_{i+1,j-1} - \varphi_{i-1,j+1} + \varphi_{i-1,j-1}}{4}$$

$$\varphi_x = \frac{\partial \varphi_{i,j}}{\partial x} = \frac{\varphi_{i+1,j} - \varphi_{i-1,j}}{2}$$

$$\varphi_y = \frac{\partial \varphi_{i,j}}{\partial y} = \frac{\varphi_{i,j+1} - \varphi_{i,j-1}}{2} \tag{9}$$

B. Dividing the image into two grossly symmetric parts

To detect a suitable axis for dividing the image into two parts, roughly symmetrical to each other with respect to the axis, the correlation method is used in the following way. Note that the tacit assumption here is that the axis of symmetry is roughly along the vertical direction.

- Find the sum of all pixels in each column of the image

$$S_1(j) = \sum_{i=1}^{M} I(i,j), \quad 1 \le j \le N \tag{10}$$

- Form a digital signal $S\tilde{}1 \equiv (S1(1), S1(2), ..., S1(N))$. Reverse the order of elements of $S\tilde{}1$ to form digital signal $S\tilde{}2$:

$$\tilde{S}_2 \equiv \left(S_1(N), S_1(N-1), \ldots, S_1(1)\right) \tag{11}$$

- Find the correlation between $S\tilde{}1$ and $S\tilde{}2$, assuming that the two signals are repeated ad infinitum with period N

$$c(k) = \sum_{j=1}^{N} \tilde{S}_1(j+k)\tilde{S}_2(j), \quad k = 1, 2, \ldots, N \tag{12}$$

with the understanding that $S\tilde{}1(j + k) = S\tilde{}1 \ (\mathrm{mod} N(j + k))$

- Shift $k*$, that corresponds to the maximum correlation ($\max\{c(k), 1 \le k \le N\}$), identifies the column that divides the image into two grossly symmetric parts.

C. Registration

After the input image has been divided into two parts, the right part is left-to-right mirrored, to facilitate the registration process. We assume that these two half images are two separate images which are taken at two successive times $t-1$ and t. To find a correspondence function T, that takes each point (x, y) in the first image and finds the corresponding point $T(x, y)$ in the second image, we use an intensity-based registration algorithm assuming an affine transformation (Periaswamya & Faridb 2006; Horn 1986; Barron et al. 1994).

By assuming an affine transformation and brightness constancy, which states that if the location of a small region changes, the image intensities in the region remain unchanged, we have:

$$I(x, y, t) = I(a_1x + a_2y + a_5, a_3x + a_4y + a_6, t-1) \tag{13}$$

To estimate parameters $\tilde{a} \equiv (a1\ a2\ a3\ a4\ a5\ a6)^T$, the method of minimising the mean squared error is used:

$$E(\vec{a}) \equiv \sum_{(x,y)\in\Omega} \left[I(x,y,t) - I(a_1x+a_2y+a_5, a_3x+a_4y+a_6, t-1)\right]^2 \tag{14}$$

where Ω denotes a spatial region of interest in the image. Parameter vector $\tilde{a}$ is chosen so that $E(\tilde{a})$ is minimal.

To simplify the minimization, this equation may be approximated by using a first order Taylor series expansion

$$\begin{aligned} E(\vec{a}) \approx \sum_{(x,y)\in\Omega} \Big(I(x,y,t) - \big[I(x,y,t) + (a_1x+a_2y+a_5-x)I_x(x,y,t) \\ + (a_3x+a_4y+a_6-y)I_y(x,y,t) - I_t(x,y,t)\big]\Big)^2 \end{aligned} \tag{15}$$

where $I_x(.)$ and $I_y(.)$ are the spatial derivatives of $I(.)$, and $I_t(.)$ is the temporal derivative of $I(.)$.

Now, this error equation may be reduced to:

$$\begin{aligned} E(\vec{a}) \approx \sum_{(x,y)\in\Omega} \Big(\big[-(a_1x+a_2y+a_5-x)I_x(x,y,t) \\ -(a_3x+a_4y+a_6-y)I_y(x,y,t) + I_t(x,y,t)\big]\Big)^2 \end{aligned} \tag{16}$$

It may also be expressed as:

$$E(\vec{a}) = \sum_{(x,y)\in\Omega} \left[k - \vec{c}^T\vec{a}\right]^2 \tag{17}$$

where, scalar $k \equiv xI_x + yI_y + I_t$ and vector $\tilde{c} \equiv (xI_x\ yI_x\ xI_y\ yI_y\ I_x\ I_y)^T$.

Now the error function may be minimised by differentiating it with respect to $\tilde{a}$

$$\frac{dE(\vec{a})}{d\vec{a}} = \sum_{(x,y)\in\Omega} (-2)c\left[k - \vec{c}^T\vec{a}\right] \tag{18}$$

So, by setting this derivative equal to zero, we have:

$$\vec{a} = \left(\sum_{(x,y)\in\Omega} \vec{c}\,\vec{c}^T\right)^{-1} \sum_{(x,y)\in\Omega} \vec{c}\,k \tag{19}$$

Then, we consider each contour, which has been identified in the first stage, as a binary image and transform the contours in the left part of the image by using the transformation parameters to identify the corresponding contour in the reference image.

D. Refinement Stage

The next step is to identify the corresponding contours. As our contours are closed curves (or curves that become closed once the image border is considered), we fill each closed contour in each half image with a unique label. Each contour is treated separately, so contours inside contours are represented in different layers as shown in Figure 1. In this figure, l_1, ..., l_6 represent distinct labels of the pixels of the corresponding regions.

Once registration of contours has been achieved, we identify for each contour the contour with which it corresponds in the other half of the image, by checking the contour with which it shares the maximum pixel overlap. To avoid contours of significantly different sizes being matched, we start by considering the contours with the largest areas.

We start by ranking the contours of both half images according to their area, in decreasing order.

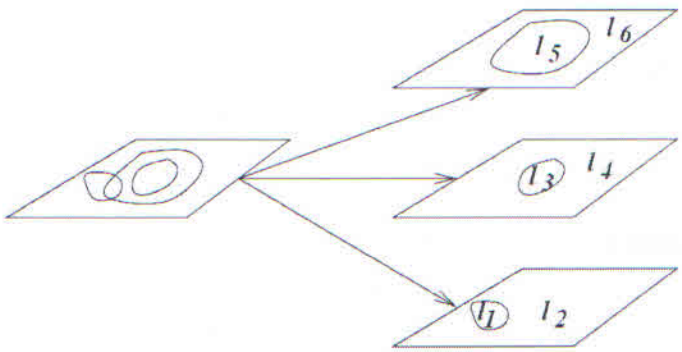

FIGURE 1. Different contours are represented in different layers

We consider the largest contour of one image, and by checking the labels of the registered contours, we identify an overlapping measure between this contour and all contours of the other half image with which it has common interior pixels after registration. Let us call A the contour we consider and Bi one of the contours of the other half image. For each pair of contours A and Bi considered, we compute an overlapping measure

$$S(A, B_i) = \frac{\#(A \cap B_i)}{\#(A) + \#(B) - \#(A \cap B_i)} \tag{20}$$

where $\#(A)$ means the area i.e. the number of pixels inside contour A. For contour A we identify its paired contour $Bi*$ to be the one that maximises $S(A, Bi)$, i.e. $i* = arg\{\max I\ S(A, Bi)\}$. Once two contours have been matched, they are removed from the stacks of contours of the two half images and the next contour in the top of the stack is considered. When one or the other stack becomes empty, the process stops.

The process may be repeated by starting with the contours of the other half-image, in case the order by which we do the matching affects the result. Pairs of contours that have been identified by both routes are considered as matched contour pairs. Note that this process takes place using the two registered parts of the image, but once a corresponding pair of contours has been identified, the processing that will follow will use the original unregistered contours. After finding the corresponding contours, the next step of this algorithm is to identify the corresponding points on each paired contour. To find which point of the first contour corresponds to which point of the second contour, shape context expressed by using log-polar histograms (Belongie et al. 2002; Scott & Nowak 2006) is used. Consider two paired contours A(p) and B(q), each represented by a set of $m\tilde{}$ and $n\tilde{}$ points respectively ($m\tilde{} \leq n\tilde{}$). The shape context of a contour point is a histogram which expresses the relation of that point to the remaining points of the contour. The histogram is built by dividing the space around that point into k bins and counting the number of points in each bin. The corresponding points of the two contours are expected to have similar histograms. The shape context of point pi of the first contour is defined by

$$h_i(k) = \#\{p \neq p_i : (p - p_i) \in bin(k), \forall p \in A\} \tag{21}$$

where $bin(k)$ is uniform in a log-polar coordinate system. Assume $\Lambda i\, j = \Lambda(pi, qj)$ is the cost of matching two points pi and qj which is defined as

$$\Lambda_{ij} = \frac{1}{2}\sum_{k=1}^{K}\frac{\left[h_i(k) - h_j(k)\right]^2}{h_i(k) + h_j(k)} \tag{22}$$

where $hi(k)$ and $hj(k)$ are the shape contexts of pi and qj, respectively.

To find the best match of contour points, the total cost of matching points is minimised:

$$\min \sum_{i=1}^{\hat{m}} \Lambda_{i,\pi(i)} \tag{23}$$

E. Symmetry point identification

We may find a local axis of symmetry between the two contours by computing the central points of the lines joining corresponding points of the contours. However, if more than one pair of points are matched along the horizontal direction, we shall extract several points along that direction that could be considered as belonging to the symmetry axis. Therefore, we present a method which uses the lateral continuity constraint to find the axis of symmetry.

In this method we formulate the problem as one of regularisation, where the symmetry axis is estimated so that its distance from the variable number of candidate points, identified in each line from the multiple contour matched points, is minimised and at the same time the variation of the position of the axis between neighbouring lines is also minimised. For this purpose, we define a cost function. Figure 2 shows a possible axis of symmetry plotted against the row index of an image. For each value of i we may have several candidate points for the axis. Let us call them $g1, g2, ..., gK(i)$. $K(i)$ may be 0, 1, ... for different values of i. These are the points identified by matching contour points along each line of the image. Let xi denote the true position of the axis along row i. We wish to define all values of xi by minimizing

$$U \equiv \sum_{i=1}^{N}\sum_{k=0}^{K(i)}\left(x_i - g_{ik}\right)^2 + \lambda\sum_{i=1}^{N-1}\left(x_i - x_{i+1}\right)^2 \tag{24}$$

where λ is a parameter that controls the amount of smoothing we impose on the axis. This is a

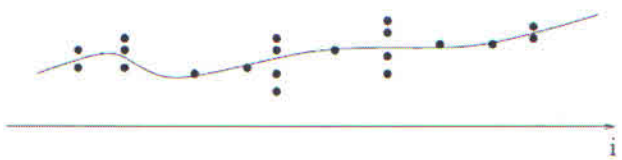

FIGURE 2. Locations of multiple symmetry points

quadratic function in the unknowns and the true position xi may be estimated by differentiating the quadratic function.

$$U \equiv \sum_{i=1}^{N}\sum_{k=0}^{K(i)}\left(x_i^2 - g_{ik}^2 - 2x_i g_{ik}\right) + \lambda\sum_{i=1}^{N-1}\left(x_i^2 - x_{i+1}^2 - 2x_i x_{i+1}\right) \tag{25}$$

$$U \equiv \sum_{i=1}^{N}\left[K(i)x_i^2 + \sum_{k=0}^{K(i)} g_{ik}^2 - 2x_i \sum_{k=0}^{K(i)} g_{ik}\right] + \lambda\sum_{i=1}^{N-1} x_i^2 + \lambda\sum_{i=1}^{N-1} x_{i+1}^2 - 2\lambda\sum_{i=1}^{N-1} x_i x_{i+1} \tag{26}$$

$\sum_{i=1}^{N} K(i)x_i^2 + \lambda\sum_{i=1}^{N-1} x_i^2$ may be written as $K(N)x_N^2 + \sum_{i=1}^{N-1}\left(\left(K(i)+\lambda\right)x_i^2\right)$, so

$$U = K(N)x_N^2 + \sum_{i=1}^{N-1}\left(\left(K(i)+\lambda\right)x_i^2\right) + \sum_{i=1}^{N}\sum_{k=0}^{K(i)} g_{ik}^2 - \sum_{i=1}^{N} 2x_i \sum_{k=0}^{K(i)} g_{ik} + \lambda\sum_{i=1}^{N-1} x_{i+1}^2 - 2\lambda\sum_{i=1}^{N-1} x_i x_{i+1} \tag{27}$$

Change variable of summation in the 5*th* term: ~$i \equiv i+1$. Then $\sum_{i=1}^{N-1} x_{i+1}^2 = \sum_{i=2}^{N} x_i^N = \sum_{i=2}^{N} x_i^2$. By rewriting $\lambda\sum_{i=1}^{N-1} x_{i+1}^2$ as $\lambda\sum_{i=2}^{N} x_i^2$ which is equal to $\lambda x_N^2 + \lambda\sum_{i=2}^{N-1} x_i^2$, and also by rewriting $\sum_{i=1}^{N-1}\left(\left(K(i)+\lambda\right)x_i^2\right)$ as $\left(K(1)+\lambda\right)x_1^2 + \sum_{i=2}^{N-1}\left(\left(K(i)+\lambda\right)x_i^2\right)$, equation (27) becomes

$$U = K(N)x_N^2 + \left(K(1)+\lambda\right)x_1^2 + \lambda x_N^2 + \sum_{i=2}^{N-1}\left(\left(K(i)+2\lambda\right)x_i^2\right) + \sum_{i=1}^{N}\sum_{k=0}^{K(i)} g_{ik} - 2\lambda\sum_{i=1}^{N-1} x_i x_{i+1} \tag{28}$$

If we define $A \equiv \sum_{i=1}^{N}\sum_{k=0}^{K(i)} g_{ik}^2$ and $B(i) \equiv \sum_{k=0}^{K(i)} g_{ik}$, then

$$U = \left(K(N)+\lambda\right)x_N^2 + \left(K(1)+\lambda\right)x_1^2 + \sum_{i=2}^{N-1}\left(\left(K(i)+2\lambda\right)x_i^2\right) + A - 2\sum_{i=1}^{N} x_i B(i) - 2\lambda\sum_{i=1}^{N-1} x_i x_{i+1} \tag{29}$$

For U to be minimum, its derivative with respect to all independent variables must be zero:

$$\frac{\partial U}{\partial x_N} = 2\left(K(N)+\lambda\right)x_N - 2B(N) - 2\lambda x_{N-1} = 0 \tag{30}$$

$$\frac{\partial U}{\partial x_1} = 2\left(K(1)+\lambda\right)x_1 - 2B(1) - 2\lambda x_2 = 0 \tag{31}$$

If i 6 = 1 and i 6 = N

$$\frac{\partial U}{\partial x_i} = 2\left(K(i)+2\lambda\right)x_i - 2B(i) - 2\lambda x_{i+2} - 2\lambda x_{i-1} = 0 \tag{32}$$

The above equations represent a set of linear equations. Therefore, these equations may be written in matrix form as

$$SX = F \Rightarrow X = S^{-1}F \mid \tag{33}$$

where S, X and F are defined as

$$S = \begin{bmatrix} K(1+)\lambda & -\lambda & 0 & \cdots & 0 \\ -k & K(2)+2\lambda & -\lambda & \cdots & 0 \\ \vdots & \vdots & \vdots & \vdots & \vdots \\ 0 & \cdots & -\lambda & K(N-1)+2\lambda & -\lambda \\ 0 & \cdots & 0 & -\lambda & K(N)+\lambda \end{bmatrix}_{N\times N} \tag{34}$$

$$X = \begin{bmatrix} x_1 \\ x_2 \\ \vdots \\ x_N \end{bmatrix}_{N\times 1} \tag{35}$$

$$F = \begin{bmatrix} B(1) \\ B(2) \\ \vdots \\ B(N) \end{bmatrix}_{N\times 1} \tag{36}$$

F. Straightening the symmetry axis and identifying the abnormalities

As noted previously, reflective symmetry is one of the main characteristics of the human body that may be used as a cue for detecting and identifying abnormalities or deformities. Therefore, to indicate any suspicious regions in the medical image, it is necessary to compare the two sides of the image divided by the extracted axis of symmetry. Moreover, to facilitate comparison of the left side with the reflected right side of the image, the local axis of symmetry may be made straight by alignment of the image pixels. The alignment can be done by shifting the pixels of each line so that the points of reflective symmetry of all image lines are aligned. Then, to identify a deformity area, the absolute difference of the left side and the reflected right side of the imaged organ is computed. Note that small misalignments along the boundaries of the various tissues may appear as differences between the two halves. To identify the significant differences, grey scale opening is used to remove thin lines from the difference image, and enhance the significant differences. Figure 3 shows the example of an image with facial trauma where the trauma region and the swelling of one side of the head are identified.

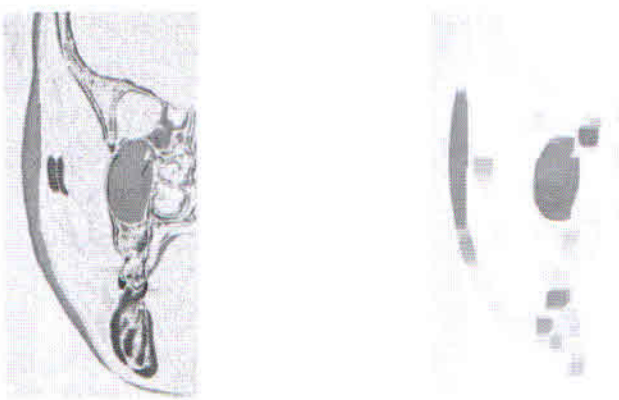

(a) (b)

FIGURE 3. (a) Absolute difference of two halves of the image of a head. The result has been scaled so white corresponds to zero difference. (b) After applying grey scale opening with a 15×15 structuring element

G. Degree of bone displacement

In some cases, the surgeons are interested in the rotation angle between the local axis of symmetry and the straightened axis of symmetry. For example, in cosmetic plastic surgery, this may help the surgeon to work out the displacement of a bony part in one side of the head in comparison with the other side. To work this

angle out, the local axis of symmetry is first fitted by a set of line segments by minimising the least square error fitting function

$$E = \sum_{i=1}^{d} [y_i - f(x_i)]^2 = \sum_{i=1}^{d} [y_i - (\alpha x_i + \beta)]^2 \tag{37}$$

where (xi, yi) are the local axis symmetry points, d is the number of points to be fitted by the line segment and $f(xi)$ is the line segment that is defined by computing coefficients α and β. The coefficients are estimated by minimising the error function E:

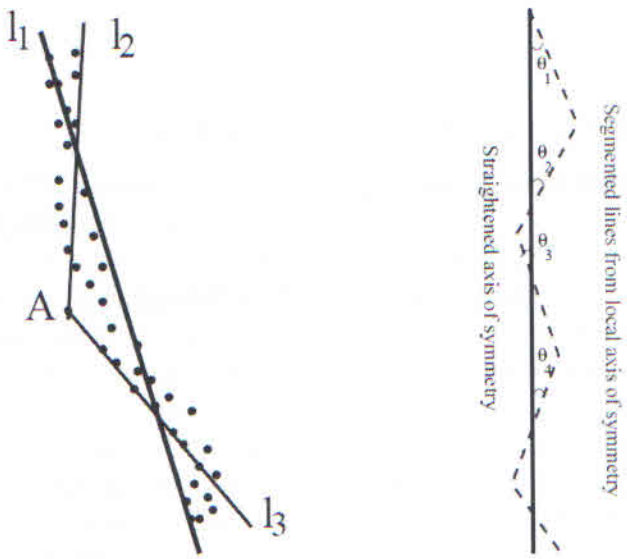

(a) (b)

FIGURE 4. (a) l_1 is a fitted line from all points, l_2 is a fitted line from all points above point A, and l_3 is a fitted line from all points below A. (b) The solid line is the straightened axis, the dashed line is a set of line segments fitting the local points of symmetry, and θ_1, θ_2 etc. are the angles between the straightened axis and the local axis of symmetry

$$\begin{bmatrix} \alpha \\ \beta \end{bmatrix} = \left(\begin{bmatrix} \sum_{i=1}^{d} x_i^2 & \sum_{i=1}^{d} x_i \\ \sum_{i=1}^{d} x_i & \sum_{i=1}^{d} 1 \end{bmatrix} \right)^{-1} \begin{bmatrix} \sum_{i=1}^{d} x_i y_i \\ \sum_{i=1}^{d} y_i \end{bmatrix} \tag{38}$$

Identifying a broken line, consisting of several line segments, that fits in the least square error sense a set of points, is an iterative process. Let us assume a set of data points as shown in Figure 4(a). The process of fitting a broken line to these points has several stages, as follows.

1) First, α and β are estimated from all the data points and all points are fitted with line l_1.
2) Then we find the point that is at maximum distance from l_1. It is point A.
3) We consider all points above A and fit line l_2 to them.
4) We consider all points below A and fit line l_3 to them.
5) We then find the point that is at maximum distance from l_2. If this distance is above a threshold, we break line l_2 to two parts, like we did with line $l1$. If not, we accept line l_2 as a good fit to its points.
6) We do the same for line l_3.

We repeat this process until all points are fitted with line segments from which they are at a distance less than the threshold.

Then, after computing all line segments, the requested angles θj are found by computing the angles between the estimated segments and the mid-straight line (see Figure 4).

RESULTS

As mentioned earlier, our algorithm consists of two parts: 1) extracting the axis of symmetry in CT images, and 2) identifying deformity areas in CT images. A total of 6 subject images (more than 1000 individual images) with different types of injury were selected for a validation study of our algorithm.

First, the algorithm was applied on a CT scan facial series (405 images) of a patient with a left orbital blowout fracture. Figure 5(a) shows some of the input images and Figure 5(b) shows the symmetry axis extracted by applying our method. The results of obtaining straight axes of symmetries after the pixel alignment process can be seen in Figure 5(c). Figure 5(d) shows the results of applying the method for identifying the deformity. The white marks show the difference between the two halves of the images which in this case correctly identify the orbital blowout fracture. To validate the extraction of the axes of symmetry method, we computed the correlation coefficient of the two halves of the input images before correction (original) and after the final alignment. The result of the comparison is shown in Figure 6.

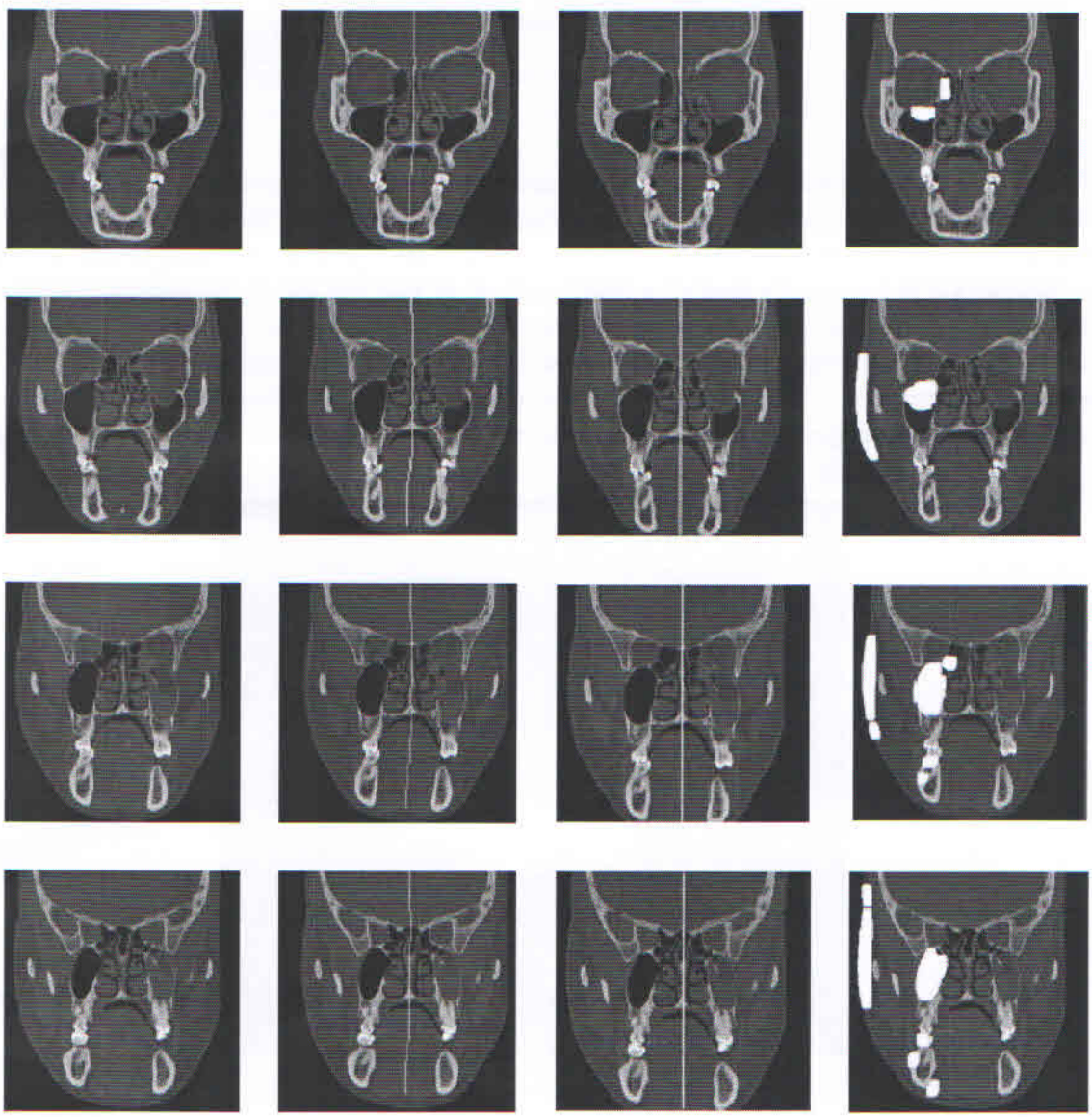

FIGURE 5. Orbital blowout fracture case (a) input images (b) local axes of symmetries (c) obtained straight axes of symmetries (d) white marks indicate suspicious areas

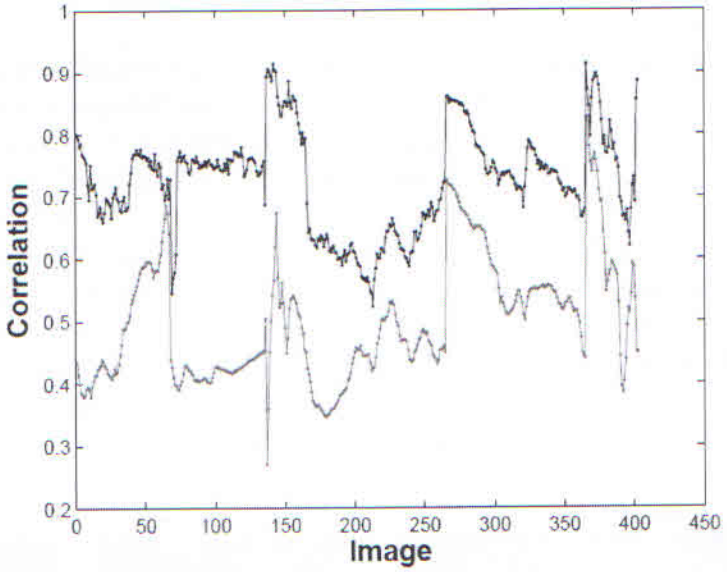

FIGURE 6. Correlation of two image halves before correction (grey) and after correction (black) for 405 test images of the first patient

The second subject was a female patient with frontotemporal osteoradionecrosis. The CT scan was taken for planning titanium cranioplasty. The 3D image of the skull of the patient is shown in Figure 7. The black arrow in the 3D image indicates the defected area. The results of our algorithm are shown in Figure 8. Figure 8(a) shows two CT images of the skull of a female patient. In 8(b), the results of applying our proposed algorithm for detecting axes of symmetries are shown. Figure 8(c) shows the straight axes of symmetries and finally, in 8(d), by the bone defected area is detected and shown in white. Also, Figure 9 shows the validation of the extraction of the axis of symmetry method by computing the correlation coefficient of the two halves of the input images before correction (original) and after the final alignment.

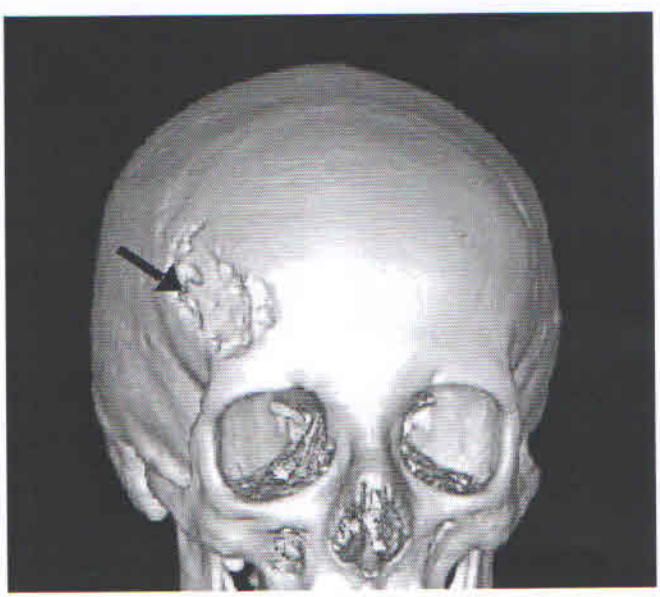

FIGURE 7. The black arrow indicates the defected area

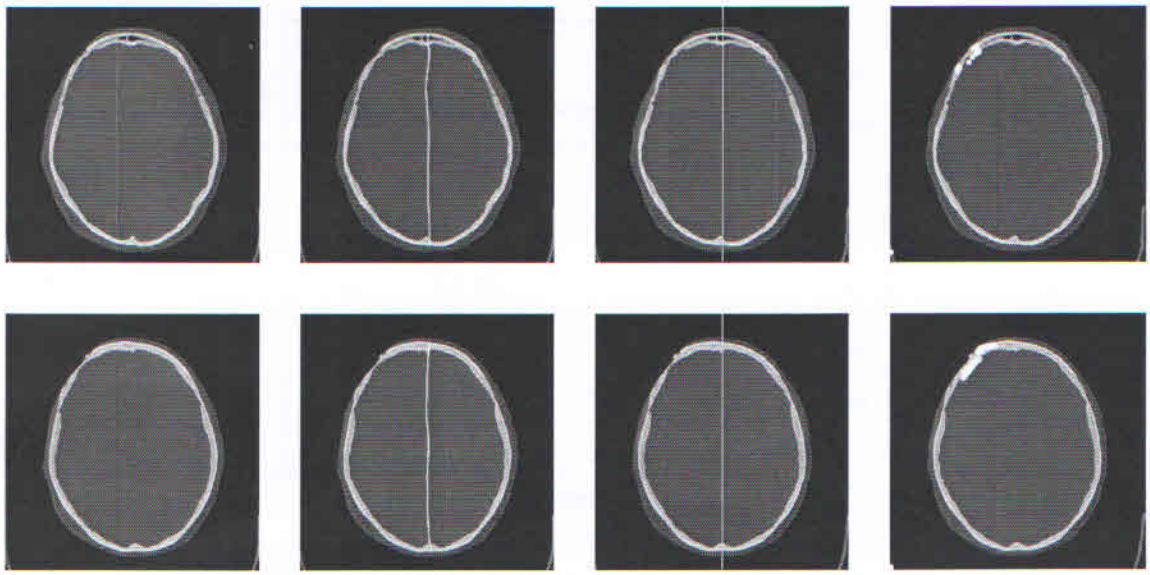

FIGURE 8. Frontotemporal bone defect case (a) input images (b) local axes of symmetries (c) obtained straight axes of symmetries (d) white marks indicate suspicious areas

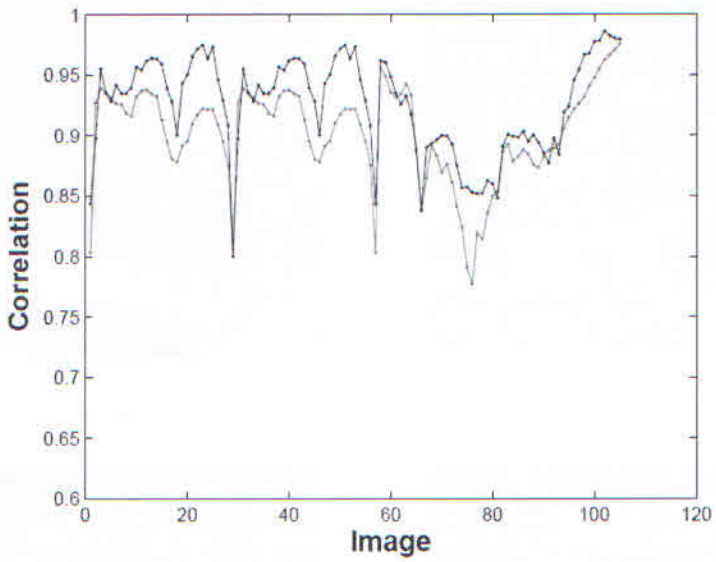

FIGURE 9. Correlation of two image halves before correction (grey) and after correction (black) for 107 test images of the second patient

Next, the algorithm was applied on a CT scan facial series of a patient with multiple fractures on his skull. Figure 11 shows the results for this patient. As it can be seen, the multiple bone fractures and soft tissue deformities are identified by the method.

The fourth case was a patient with a Nasal bone fracture. Figure 12 shows the results for this case. In addition, the results of the validation process can be seen in Figure 13.

Fronto orbital neurofibromatosis case was the fifth case that our algorithm was applied to.The results are shown in Figures 15 and 14.

Finally, our algorithm was applied to a normal case. The results are shown in Figures 15 and 16.

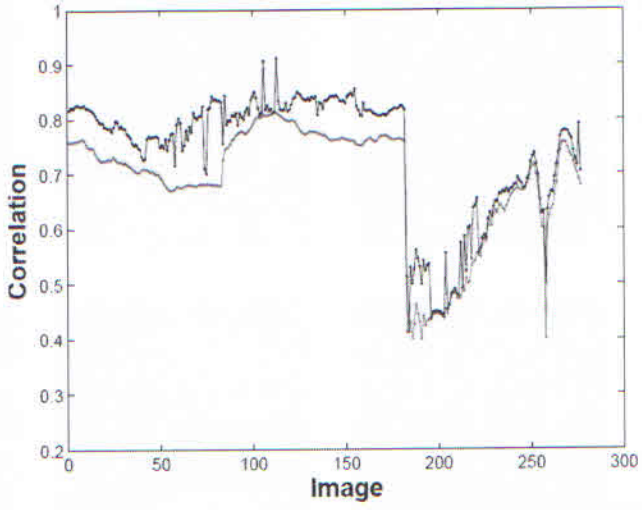

FIGURE 10. Correlation of two image halves before correction (grey) and after correction (black) for the third patient CT images

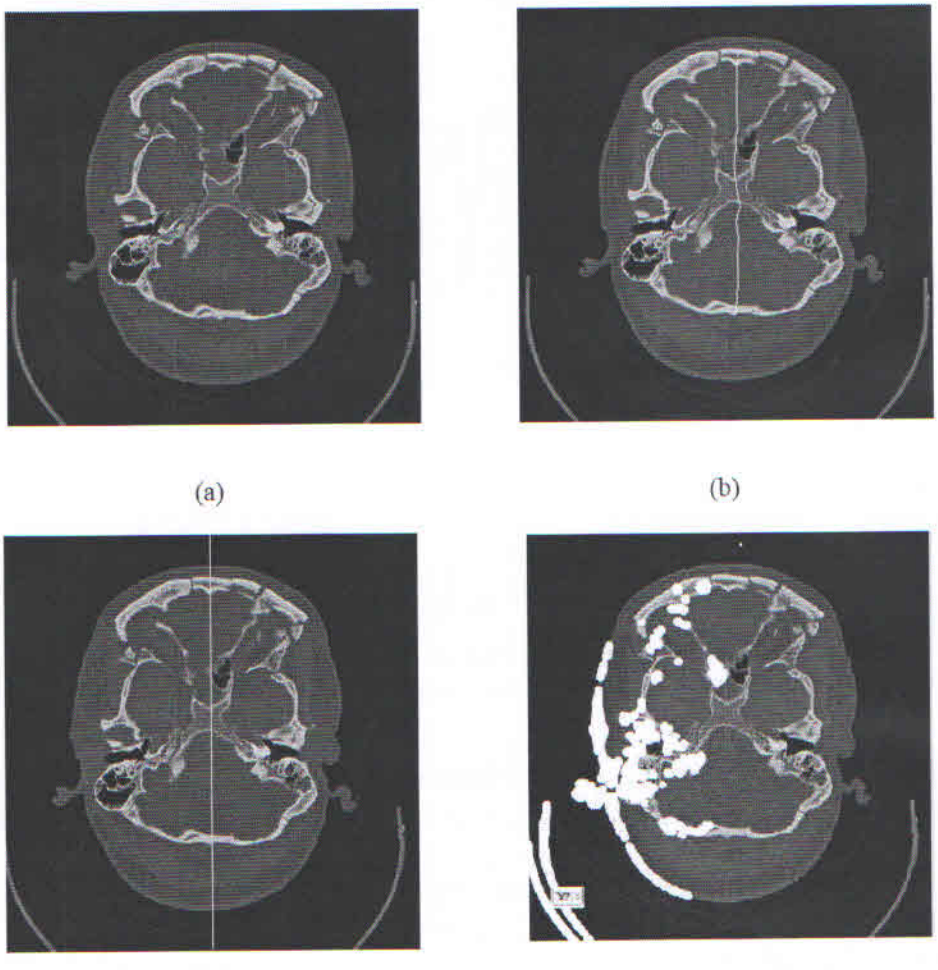

(a) (b)

(c) (d)

FIGURE 11. Multiple fractures case (a) input image (b) local axis of symmetry (c) obtained straight axis of symmetry (d) white marks indicate suspicious areas

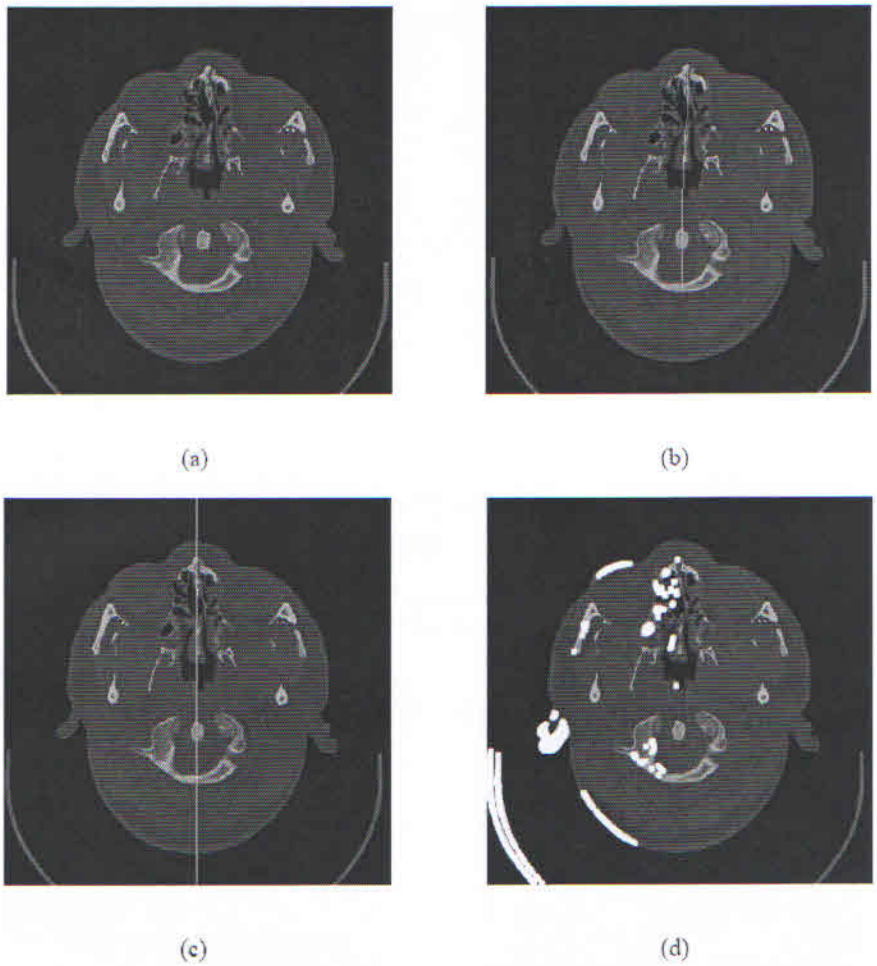

(a) (b)

(c) (d)

FIGURE 12. Nasal bone fracture case (a) input image (b) local axis of symmetry (c) obtained straight axis of symmetry (d) white marks indicate suspicious areas

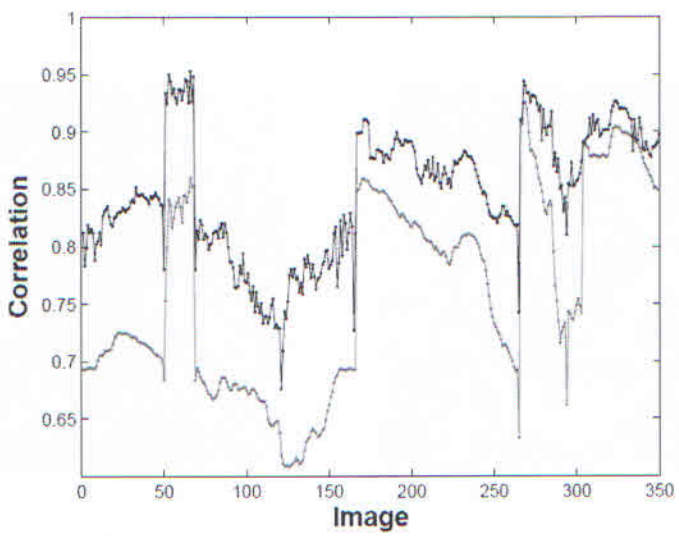

FIGURE 13. Correlation of two image halves before correction (grey) and after correction (black) for CT images of the fourth patient

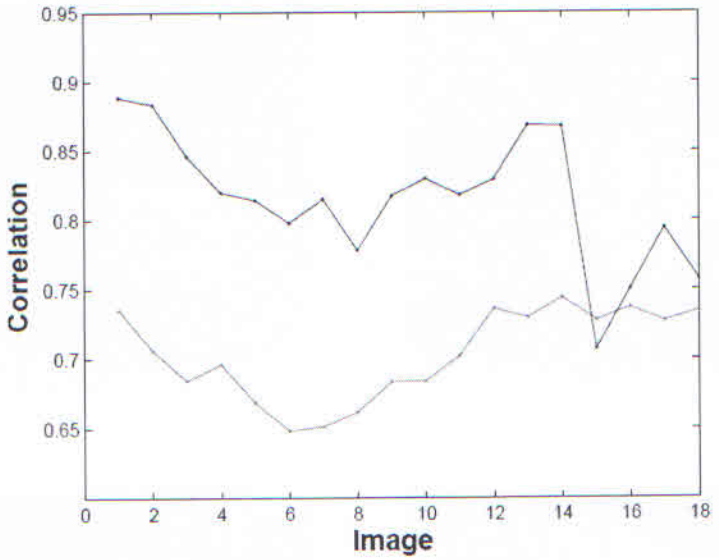

FIGURE 14. Correlation of two image halves before correction (grey) and after correction (black) for CT images of the fifth patient

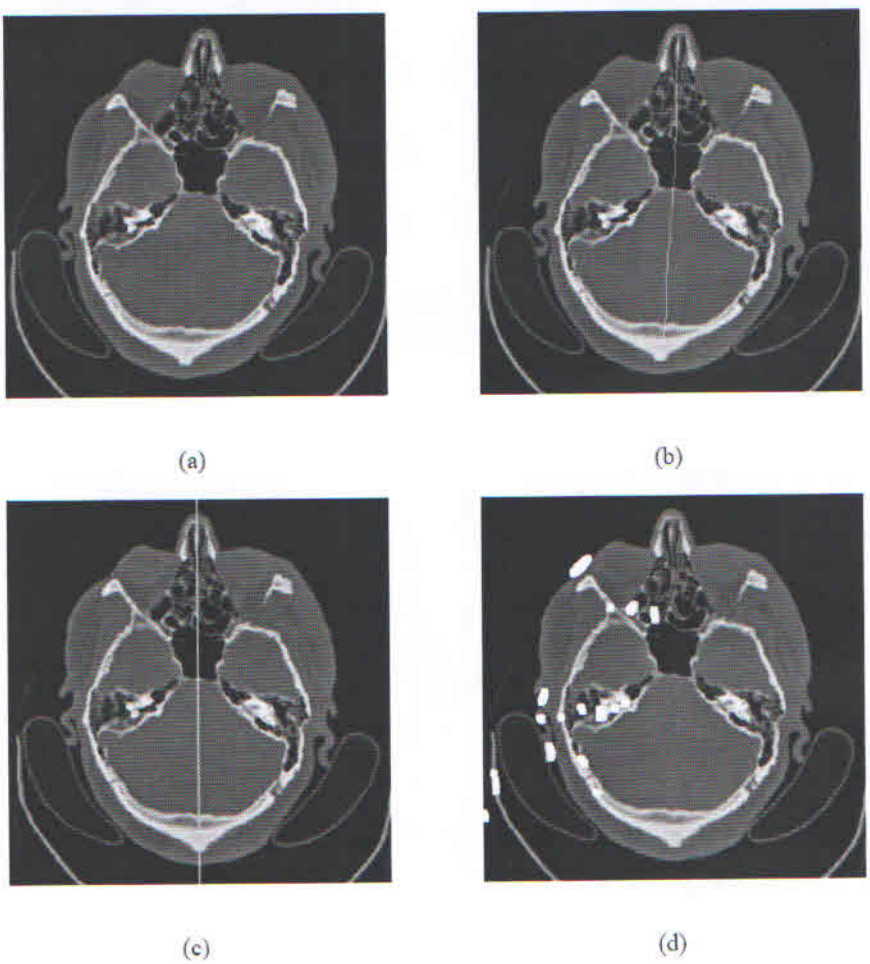

FIGURE 15. Fronto orbital neurofibromatosis case (a) input images (b) local axis of symmetry (c) obtained straight axis of symmetry (d) white marks indicate suspicious areas

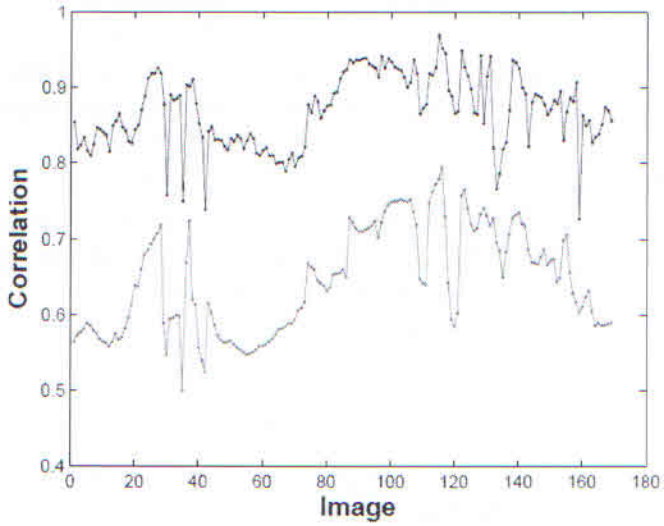

FIGURE 16. Correlation of two image halves before correction (grey) and after correction(black) for CT images of the normal person.

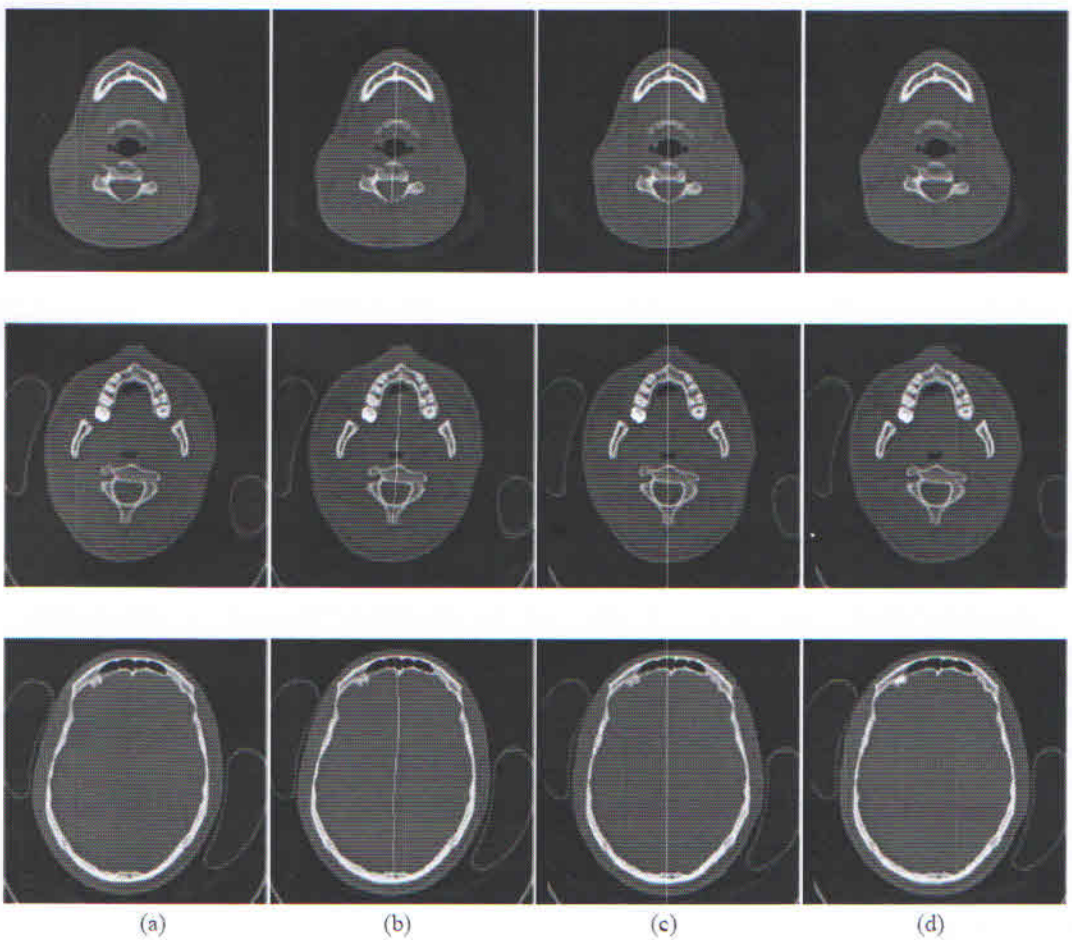

FIGURE 17. Normal case (a) input images (b) local axis of symmetry (c) obtained straight axis of symmetry (d) white marks indicate suspicious areas

DISCUSSION AND CONCLUSIONS

We presented some generic methodology for defining a generalised symmetry axis in medical images. After detecting the symmetry axis, the difference between the two halves of the imaged organ were quantified. The only assumption we made was that the axis was roughly vertical.

This however, is not particularly restrictive, as frontal imaging produces such images and in any case images may be rotated prior to using our algorithm to comply with this assumption. The application we have in mind is plastic surgery for correcting bone deformations. However, our algorithm is also useful for finding defected soft tissues. Our method was applied to 1000 images and the detected deformation areas agreed with the doctor's diagnosis, in each case.

ACKNOWLEDGMENTS

This work was supported by the portfolio grant "Integrated Electronics". We are grateful to Prof Niall Kirkpatrick for supplying the data and the diagnosis for each patient.

REFERENCES

Alterson, R. & Plewes, D. B. 2003. Bilateral symmetry analysis of breast MRI, *Physics in Medicine and Biology* 48: 3431-3443.

Barron, J. L., Fleet, D. J. & Beauchemin, S. S. 1994. Performance of optical flow techniques, *International Journal of Computer Vision* 12: 43-77.

Belongie, S., Malik, J. & Puzicha, J. 2002. Shape matching and object recognition using shape contexts, *IEEE Transactions on Pattern Analysis and Machine Intelligence* 24: 509-522.

Bonneh, Y., Reisfeld, D. & Yeshurun, Y. 1993. Texture discrimination by local generalized symmetry, *Proceedings of Fourth International Conference on Computer Vision*: 461-465.

Chan, T. F. & Vese, L. A. 2001. Active contours without edges, *IEEE Transactions on Image processing* 10: 266-277.

Chetverikov. 1995. Pattern Orientation and Texture Symmetry, *Proceedings of the 6th International Conference on Computer Analysis of Images and Patterns*: 222-229.

Horn, K. P. 1986. *Robot Vision*, Cambridge, MA: MIT Press.

Joshi, S., Lorenzen, P., Gerig, G. & Bullitt, E. 2003. Structural and radiometric asymmetry in brain images, *Mathematical Methods in Biomedical Image Analysis* 7: 155-170.

Junck, L., Moen, J. G., Hutchins, G. D., Brown, M. B. & Kuhl, D. E. 1990. Correlation methods for the Centering, rotation, and alignment of functional brain images, *The Journal of Nuclear Medicine* 31: 1220-1226.

Mancas, M., Gosselin, B. & Macq, B. 2005. Fast and automatic tumoral area localisation using symmetry, *Proceedings of the IEEE International Conference on Acoustics, Speech, and Signal Processing (ICASSP)* 2: 725-728.

Mitra, S. & Liu, Y. 2004. Local facial asymmetry for expression classification,*Proceedings of the 2004 IEEE Conference on Computer Vision and Pattern Recognition* 2: 889-894.

Mumford & Shah, J. 1989. Optimal approximation by piecewise smooth functions and associated variational problems, *Communication on Pure and Applied Mathematics* 42: 577-685.

Osher, S. & Fedkiw, R. 2002. *Level Set Methods and Dynamic Implicit Surfaces*, New York: Springer.

Periaswamya S. & Faridb H. 2006. Medical image registration with partial data, *Medical Image Analysis* 10: 452-464.

Prima, S., Ourselin, S. & Ayache, N. 2002. Computation of the mid-sagittal plane in 3-D brain images, *IEEE transactions onmedical imaging* 21: 122-38.

Scott & Nowak, R. 2006. Robust contour matching via the order-preserving assignment problem, *IEEE Transactions on Image Processing*, 15: 1831-1838.

Tuzikov, V., Colliot, O. & Bloch I. 2003. Evaluation of the symmetry plane in 3D MR brain images, *Pattern recognition letters* 24: 2219-2233.

Zielke, T., Brauckmann, M. & von Seelen, W. 1993. Intensity and edge-based symmetry detection with an application to carfollowing, *CVGIP: Image Understanding* 58: 177-190.

Maria Petrou
Director of ITI
Centre for Research and Technology Hellas (CERTH)
6km Harilaou-Thermi, P.O. Box 60361
Thessaloniki, 57001, Greece
http:www.iti.gr/~petrou